

# Study of the reactions $\gamma p \rightarrow K^+ \Sigma^\pm \pi^\mp$ at photon energies up to 2.6 GeV\*

I. Schulday<sup>1,3a</sup>, R. Lawall<sup>1,5</sup>, J. Barth<sup>1</sup>, K.-H. Glander<sup>1,4</sup>, S. Goers<sup>1,5</sup>, J. Hannappel<sup>1</sup>, N. Jöpen<sup>1</sup>, F. Klein<sup>1,b</sup>, E. Klempt<sup>2</sup>, D. Menze<sup>1</sup>, E. Paul<sup>1</sup>, W.J. Schuille<sup>1</sup>

<sup>1</sup> Physikalisches Institut der Universität Bonn, Germany

<sup>2</sup> Helmholtz-Institut für Strahlen- und Kernphysik, Universität Bonn, Germany

<sup>3</sup> presently IFB AG, Köln, Germany

<sup>4</sup> presently TRW Automotive GmbH, Alfdorf, Germany

<sup>5</sup> presently TÜV Nord, Hamburg, Germany

Received: date / Revised version: date

**Abstract.** The reactions  $\gamma p \rightarrow K^+ \Sigma^\pm \pi^\mp$  were studied with the SAPHIR detector using a tagged photon beam at the electron stretcher facility ELSA in Bonn. The decays  $\Sigma^- \rightarrow n\pi^-$  and  $\Sigma^+ \rightarrow n\pi^+, p\pi^0$  were fully reconstructed. Reaction cross sections were measured as a function of the photon energy from threshold up to 2.6 GeV with considerably improved statistics compared to a previous bubble chamber measurement. The cross sections rise monotonously with increasing photon energy. The two-particle mass distributions of  $\Sigma^\pm \pi^\mp$  and  $K^+ \pi^-$  show substantial production of resonant states.

**PACS.** 13.30.-a Decays of baryons – 14.20.Jn hyperons

## 1 Introduction

Photon-induced reactions on nucleons at low energies are commonly used to study the excitation of baryonic resonances. A review of baryon spectroscopy, its aims and its achievements can be found elsewhere [1]. Searches for such resonances were carried out in the SAPHIR experiment analysing the reactions  $\gamma p \rightarrow K^+ \Lambda$  [2],  $\gamma p \rightarrow K^+ \Sigma^0$  [3],  $\gamma p \rightarrow K^0 \Sigma^+$  [4],  $\gamma p \rightarrow \varrho p$  [5],  $\gamma p \rightarrow \omega p$  [6],  $\gamma p \rightarrow \Phi p$  [7], and  $\gamma p \rightarrow \eta' p$  [8]. The measurements presented here extend this search to the reactions  $\gamma p \rightarrow K^+ \Sigma^\pm \pi^\mp$  where strangeness-zero resonant states might contribute.

The data analysis is based on 180 million triggered events which were taken with the magnetic multiparticle detector SAPHIR [9] at the 3.5 GeV electron stretcher facility ELSA [10] using a tagged photon beam which covered the photon energy range from threshold (of the reactions considered here) to 2.6 GeV. A detailed description of the experiment is given elsewhere [2, 6].

The data are available via internet<sup>1</sup>.

\* This work is supported in part by the Deutsche Forschungsgemeinschaft (SPP KL 980/2-3) and the SFB/TR16

<sup>a</sup> Part of doctoral thesis (I. Schulday, doctoral thesis, Bonn University (2004), Bonn-IR-2004-15), <http://saphir.physik.uni-bonn.de/saphir/thesis.html>

<sup>b</sup> email: [klein@physik.uni-bonn.de](mailto:klein@physik.uni-bonn.de)

<sup>1</sup> <http://saphir.physik.uni-bonn.de/saphir/publications>

## 2 Event reconstruction and event selection

The kinematical reconstruction of the reactions  $\gamma p \rightarrow K^+ \Sigma^- \pi^+$  with  $\Sigma^- \rightarrow n\pi^-$ , and of  $\gamma p \rightarrow K^+ \Sigma^+ \pi^-$  with either  $\Sigma^+ \rightarrow n\pi^+$  or  $\Sigma^+ \rightarrow p\pi^0$ , was based on the measurements of the photon energy in the tagging system and of the three-momenta of the charged particles in the final states reconstructed in the drift chamber system. The topology of the events is sketched in fig. 1.

In the first step, the primary vertex was searched by combining pairs out of the three tracks extrapolated into the target region. The pair with the best matching was accepted. Then the hypotheses  $\gamma p \rightarrow K^+ \Sigma^\pm \pi^\mp$  were tested by a kinematical fit which used the photon energy and the reconstructed momenta of  $K^+$  and  $\pi^\mp$ . The hypothesis with the better fit probability were tested by a kinematical fit which used the photon energy and the reconstructed momenta of the particles defining the primary vertex. The fit determined the 3-momentum of the  $\Sigma^\pm$  which allowed us to reconstruct its track downstream of the accepted primary vertex. In the next step, the  $\Sigma^\pm$  decay vertex was calculated as intercept of the  $\Sigma^\pm$  track with the extrapolated track of the third charged particle. The decay hypotheses  $\Sigma^- \rightarrow n\pi^-$  and  $\Sigma^+ \rightarrow p\pi^0/n\pi^+$  were tested at the decay vertex by carrying out corresponding kinematical fits, and the complete reaction was tested by simultaneous fits at both, the primary and the decay vertex. Finally, time-of-flight (TOF) measurements carried out in the range of the geometrical acceptance of the scintillator hodoscopes were used to reject background

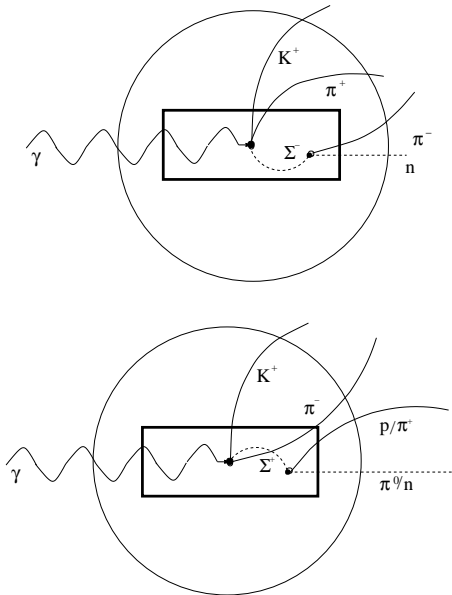


**Fig. 1.** Topologies of the reactions  $\gamma p \rightarrow K^+ \pi^+ \Sigma^-$  (top) and  $\gamma p \rightarrow K^+ \pi^- \Sigma^+$  (bottom) in the target region. Rectangle and circle represent the target area and the inner layer of the central drift chamber. The  $\Sigma^\pm$  track was not measured.

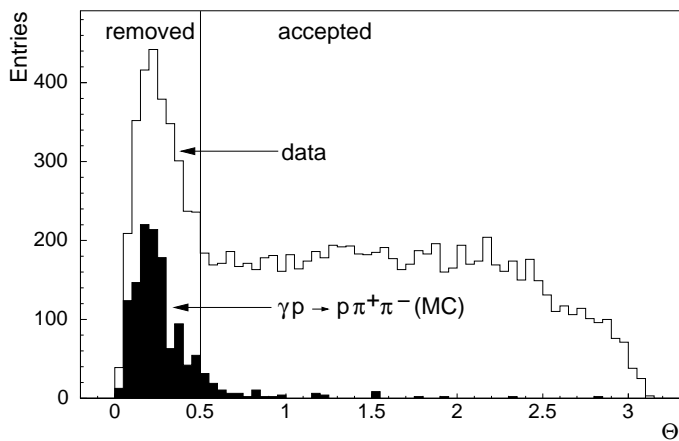


**Fig. 2.** Angular distribution of the decay proton in the  $\Sigma^+$  rest system for the decay  $\Sigma^+ \rightarrow p \pi^0$  for data and Monte Carlo simulated background of events from the reaction  $\gamma p \rightarrow p \pi^+ \pi^-$  (black area) which passed the selection cuts. The Monte Carlo event sample was normalised to the photon flux. The vertical line indicates the cut which was applied to exclude most of this background.

from other reactions. For  $\gamma p \rightarrow K^+ \Sigma^- \pi^+$  it was required that the mass assignments, obtained from TOF measurements for the positively charged particles, had a value below 0.8 GeV. This cut removed events with a proton in the final state. For  $\gamma p \rightarrow K^+ \Sigma^+ \pi^-$  it was required that the mass assignments were consistent with the mass values from the fit.

At this stage, the sample of events identified as  $\gamma p \rightarrow K^+ \Sigma^+ \pi^-$  with  $\Sigma^+ \rightarrow p \pi^0$  still contained substantial background from events due to the reaction  $\gamma p \rightarrow p \pi^+ \pi^-$ . The final states of these reactions have proton and  $\pi^-$

in common, and the identification of pions and kaons is not unique because of the limited time resolution of the time-of-flight (TOF) measurement and the restriction of geometrical acceptance of the scintillator hodoscopes.

Figure 2 shows the proton angular distribution in the  $\Sigma^+$  rest system with respect to the momentum of  $\Sigma^+$  in the laboratory system. For comparison, the same distribution of Monte-Carlo simulated events due to  $\gamma p \rightarrow p \pi^+ \pi^-$  is shown which passed the same selection cuts. The peak in the data at low angles is qualitatively described by the simulated background. An angular cut was applied (vertical line) to remove most of this background contribution. In the next step, the decay time of  $\Sigma^\pm$  was calculated using the track length and the 3-momentum of the  $\Sigma^\pm$ . The distributions are shown in figs. 3 and 4 together with those of Monte-Carlo simulated events. The residual background seen at large decay times is due to secondary reactions in target and central drift chamber. It is subtracted in the final background subtraction.

The strong excess of events at small decay times indicates background from other reactions which accumulates at small times. Due to the limited resolution this is expected if all charged particles originate from the same production vertex. In order to reduce this background, events with  $t_{\Sigma^\pm} < 0.7 \cdot 10^{-10}$  s were removed. For events with  $\Sigma^+$  decay, another cut was applied for large decay times. The cut  $t_{\Sigma^+} > 4.5 \cdot 10^{-10}$  s removed events in a region where further background is visible.

The data sets, obtained after the selection cuts, contained 4429 events from the reaction  $\gamma p \rightarrow K^+ \Sigma^- \pi^+$  and 11267 events from  $\gamma p \rightarrow K^+ \Sigma^+ \pi^-$ , with 5080 of the  $\Sigma^+$  decaying into  $n \pi^+$  and 6187 into  $p \pi^0$ . Background contributions which were not removed by the selection cuts described above were estimated by Monte-Carlo simulations and finally subtracted (section 6).

### 3 Acceptance of the events

The acceptance was determined by simulating events in the SAPHIR setup for the reactions  $\gamma p \rightarrow K^+ \Sigma^\pm \pi^\mp$  according to phase space with propagation of  $\Sigma^\pm$  and subsequent decays  $\Sigma^- \rightarrow n \pi^-$  and  $\Sigma^+ \rightarrow p \pi^0$  or  $\Sigma^+ \rightarrow n \pi^+$ , respectively. Charged particles in the final states were tracked through the drift chamber system taking into account the magnetic field and multiple scattering in all materials. Simulated events were processed like real events through the event reconstruction and selection procedures. The total acceptance accounted for the trigger efficiency of the data taking periods, the event reconstruction efficiency and the data reduction according to the event selection cuts. The mean acceptance was of the order of 10% for  $\gamma p \rightarrow K^+ \Sigma^- \pi^+$  and 2% for  $\gamma p \rightarrow K^+ \Sigma^+ \pi^-$ . The acceptance of the latter reaction was lower because it includes the efficiency of the TOF measurements for both  $\Sigma^+$  decay modes and, in addition, the cut in the angular distribution of  $\Sigma^+ \rightarrow p \pi^0$  decays (see section 2).

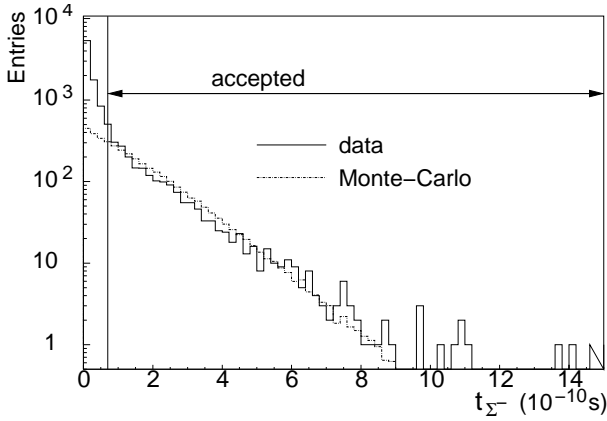


**Fig. 3.** Decay time distribution of the  $\Sigma^-$  for data (solid line) and for Monte Carlo simulated events (dashed line), normalised to the data in the accepted area. The vertical line indicates the cut applied to the data.

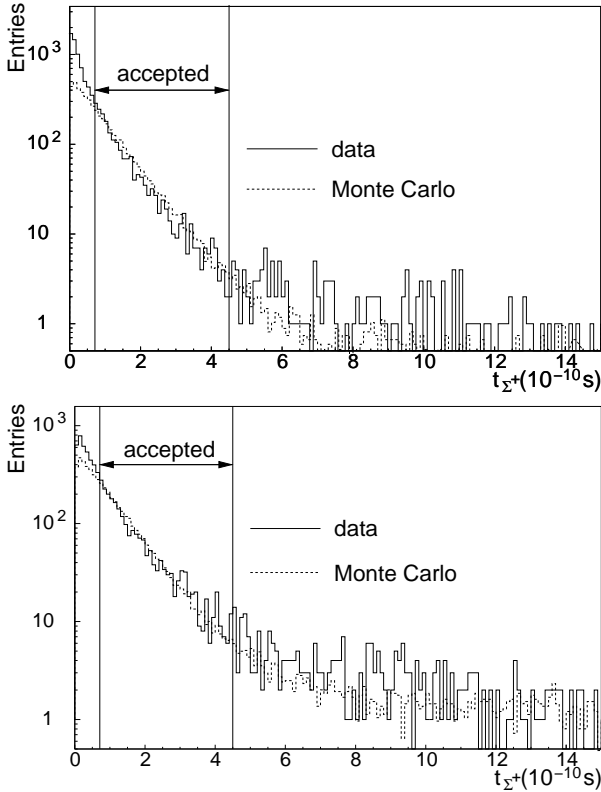


**Fig. 4.** Top: Decay time distribution of the  $\Sigma^+$  with decay  $\Sigma^+ \rightarrow n\pi^+$  for data (solid line) and Monte Carlo simulated events (dashed line), normalised to the data in the accepted area. Bottom: Decay time distribution of the  $\Sigma^+$  with decay  $\Sigma^+ \rightarrow p\pi^0$  for data (solid line) and Monte Carlo simulated events (dashed line), normalised to the data in the accepted area. The vertical lines indicate the cuts applied to the data.

## 4 Background from other reactions

Background was estimated by generating events according to phase space for the reactions listed in table 1. The events were processed through reconstruction and selec-

tion criteria as real events. The background event samples obtained were normalised according to the photon flux.

The errors in the background estimate are dominated by a constant value of 10% due to the model dependence of the event simulation and the uncertainty of the background cross sections. This error and the statistical errors were added in quadrature. For  $\gamma p \rightarrow K^+ \Sigma^\pm \pi^\pm$ ,  $\Sigma^\pm \rightarrow n\pi^\mp$ , the reactions  $\gamma p \rightarrow p\pi^+\pi^-\pi^0$  and  $\gamma p \rightarrow n\pi^+\pi^+\pi^-$  contribute on average with about 10%, and all reactions together with  $(13 \pm 1.4)\%$  to the observed total cross section (see section 6). For  $\gamma p \rightarrow K^+ \Sigma^+ \pi^-$ ,  $\Sigma^+ \rightarrow p\pi^0$ , the reaction  $\gamma p \rightarrow p\pi^+\pi^-$  contributes on average with about 10% and the total background adds up to  $(20 \pm 3)\%$  of the observed cross section.

**Table 1.** Reactions and cross sections in the photon energy range considered. The list includes  $\gamma p \rightarrow K^+ \Sigma^\pm \pi^\mp$ , since these reactions also contaminate each other.

Reaction	$\sigma$ [ $\mu\text{b}$ ]
$\gamma p \rightarrow n\pi^+\pi^+\pi^-$	2-10
$\gamma p \rightarrow p\pi^+\pi^-\pi^0$	5-25
$\gamma p \rightarrow p\pi^+\pi^-$	58-30
$\gamma p \rightarrow K^+ \Sigma^- \pi^+$	0-0.3
$\gamma p \rightarrow K^+ \Sigma^+ \pi^-$	0-0.7
$\gamma p \rightarrow K^+ \Lambda \pi^0$	< 1
$\gamma p \rightarrow K_S^0 \Lambda \pi^+$	< 1
$\gamma p \rightarrow K_L^0 \Lambda \pi^+$	< 1
$\gamma p \rightarrow K_S^0 \Sigma^+ \pi^0$	< 1
$\gamma p \rightarrow K^+ \Lambda$	1.8-0.6
$\gamma p \rightarrow K^+ \Sigma^0$	2.3-0.6
$\gamma p \rightarrow K^+ \Lambda \pi^+ \pi^-$	$\ll 1$
$\gamma p \rightarrow K^+ \Sigma^0 \pi^+ \pi^-$	$\ll 1$

## 5 $\Sigma\pi$ and $K\pi$ mass distributions

The invariant mass distributions for the  $\Sigma\pi$  system for the reactions  $\gamma p \rightarrow K^+ \Sigma^- \pi^+$  and  $\gamma p \rightarrow K^+ \Sigma^+ \pi^-$  are shown in figs. 5 and 6. Both,  $\Sigma^+ \pi^-$  and  $\Sigma^- \pi^+$  distributions show a peak structure in the mass range of  $\Sigma(1385)$  and  $\Lambda(1405)$  and another pronounced peak in the mass range of  $\Lambda(1520)$ . Figure 7 shows the  $K^+ \pi^-$  mass distribution for events assigned to the reaction  $\gamma p \rightarrow K^+ \Sigma^+ \pi^-$ . The peak at 890 MeV indicates  $K^{*0}$  production.

From the observed resonance peaks it can be concluded that substantial parts of both reaction cross sections are due to intermediate two-body resonant states. The  $\Lambda(1520)$  production was studied in detail and is presented in a separate paper [11].

## 6 Reaction cross sections

Cross sections were determined as a function of the photon energy for both reactions, in case of  $\gamma p \rightarrow K^+ \Sigma^+ \pi^-$  separately for both  $\Sigma^+$  decay modes.

Figures 8, 9 and 10 show the excitation function before background subtraction with statistical errors together

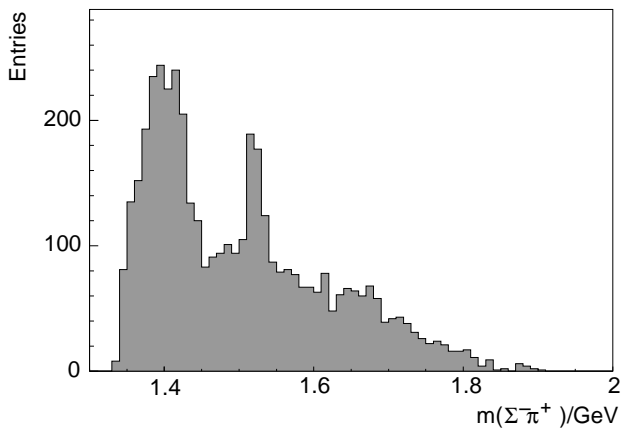


Fig. 5.  $\Sigma^- \pi^+$  invariant mass distribution.

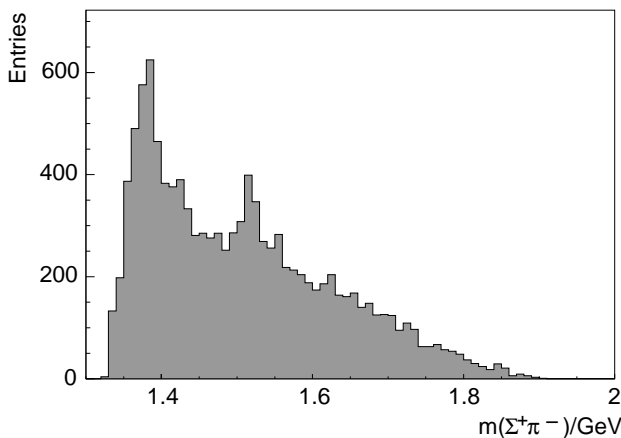


Fig. 6.  $\Sigma^+ \pi^-$  invariant mass distribution.

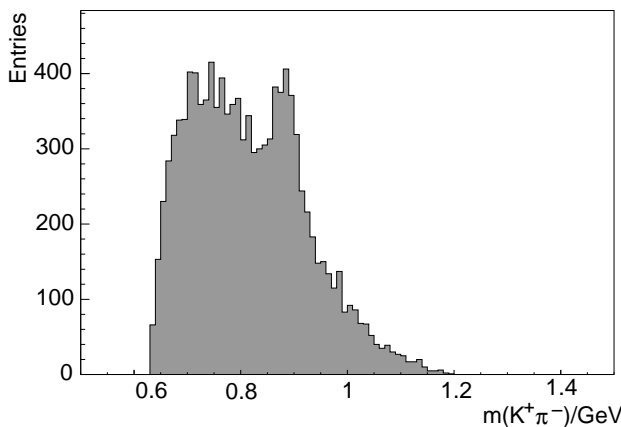


Fig. 7.  $K^+ \pi^-$  invariant mass distribution.

with the total background contributions according to section 4.

The final reaction cross sections were obtained by subtracting the accumulated background cross sections bin-by-bin. They are shown in figs. 11 and 12. The errors were calculated by quadratic addition. Cross sections and errors are quoted in tables 2, 3, and 4, respectively.

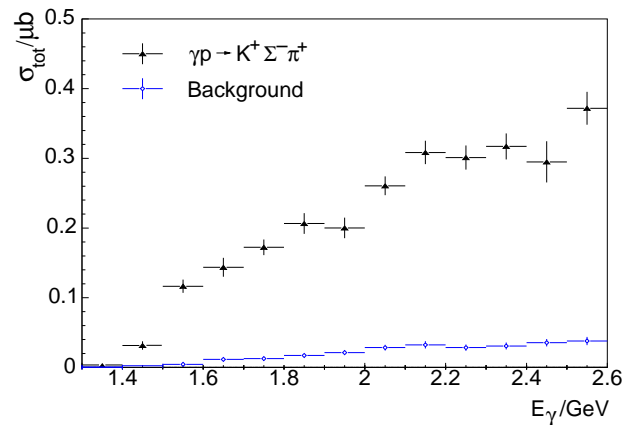


Fig. 8. Excitation function before background subtraction for  $\gamma p \rightarrow K^+ \Sigma^- \pi^+$  and background from other reactions.

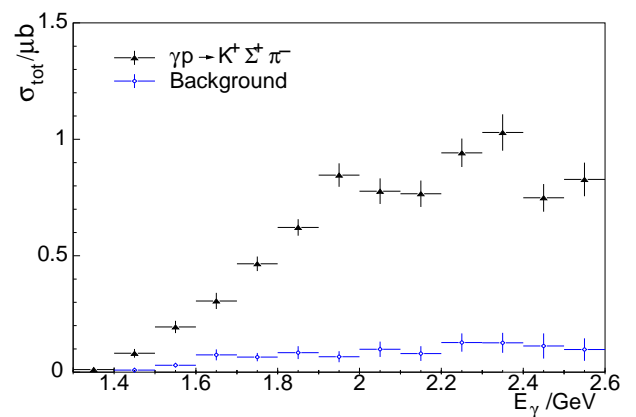


Fig. 9. Excitation function before background subtraction for the reaction  $\gamma p \rightarrow K^+ \Sigma^+ \pi^-$  with decay  $\Sigma^+ \rightarrow n \pi^+$  and background from other reactions.

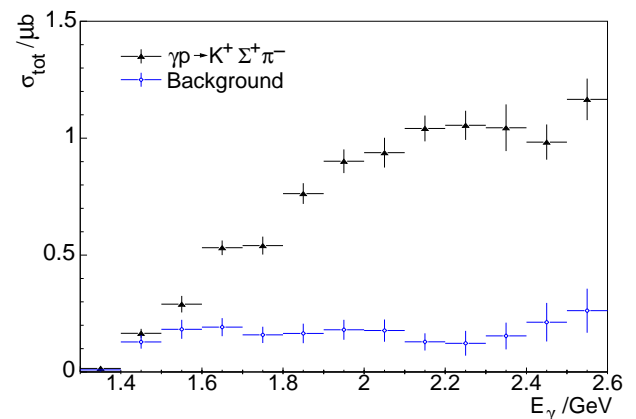
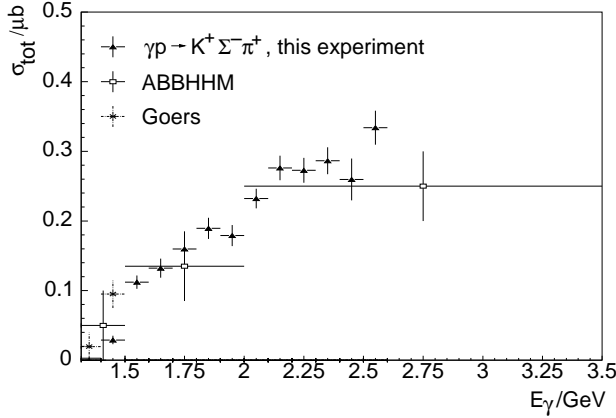


Fig. 10. Excitation function before background subtraction for the reaction  $\gamma p \rightarrow K^+ \Sigma^+ \pi^-$  with decay  $\Sigma^+ \rightarrow p \pi^0$  and background from other reactions.

## 7 Summary

The cross sections of the reactions  $\gamma p \rightarrow K^+ \Sigma^\pm \pi^\mp$  were measured in the photon energy range from threshold to 2.6 GeV. They rise monotonously up to values of about



**Fig. 11.** Cross section of the reaction  $\gamma p \rightarrow K^+ \Sigma^- \pi^+$  as a function of the photon energy after subtraction of background from other reactions in comparison to previous measurements [12, 13].

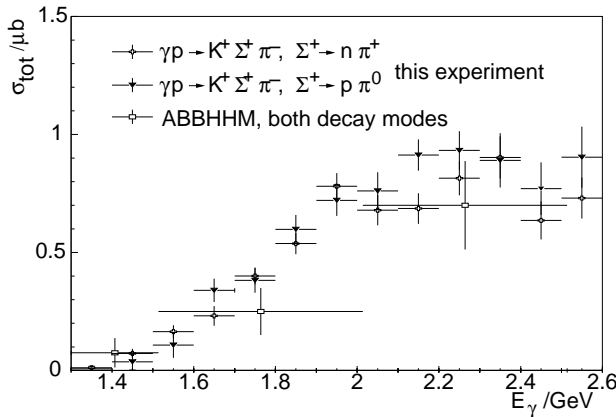


**Fig. 12.** Cross section of the reaction  $\gamma p \rightarrow K^+ \Sigma^+ \pi^-$  as a function of the photon energy after background subtraction from other reactions in comparison to previous measurements [12]. For this experiment the cross sections from both  $\Sigma^+$  decay modes are given separately.

$0.3 \mu\text{b}$  for  $K^+ \Sigma^- \pi^+$  and about  $0.8 \mu\text{b}$  for  $K^+ \Sigma^+ \pi^-$ . Regarding the hitherto existing data an evident improvement concerning the energy resolution and the total errors is achieved. No indications are found for narrow structures in the total cross sections, nor strong threshold enhancements as seen, e. g., in  $\gamma p \rightarrow p\eta$  [14],  $\gamma p \rightarrow \Lambda K^+$  [2, 15, 16], or  $\gamma p \rightarrow \omega p$  [6]. The  $\Sigma\pi$  and  $K\pi$  mass spectra show pronounced peak structures, indicating that a substantial part of the cross sections is due to two-body intermediate states. The  $\Lambda(1520)$  intermediate state is investigated in a separate paper.

## 8 Acknowledgements

We would like to thank the technical staff of the ELSA machine group for their invaluable contributions to the experiment. We gratefully acknowledge the support by the Deutsche Forschungsgemeinschaft in the framework of the Schwerpunktprogramm ‘‘Investigation of the hadronic

**Table 2.** Total cross sections of the reaction  $\gamma p \rightarrow K^+ \Sigma^- \pi^+$  for 13 bins of  $E_\gamma$ , obtained after background subtraction.

$E_\gamma$ [GeV]	$\sigma_{tot}$ [ $\mu\text{b}$ ]	$\delta\sigma$ [ $\mu\text{b}$ ]
1.300 – 1.400	0.0028	$\pm 0.0026$
1.400 – 1.500	0.0290	$\pm 0.0061$
1.500 – 1.600	0.1121	$\pm 0.0095$
1.600 – 1.700	0.1322	$\pm 0.0137$
1.700 – 1.800	0.1597	$\pm 0.0113$
1.800 – 1.900	0.1894	$\pm 0.0152$
1.900 – 1.000	0.1790	$\pm 0.0152$
2.000 – 1.100	0.2322	$\pm 0.0141$
2.100 – 2.200	0.2761	$\pm 0.0177$
2.200 – 2.300	0.2727	$\pm 0.0179$
2.300 – 2.400	0.2865	$\pm 0.0194$
2.400 – 2.500	0.2595	$\pm 0.0300$
2.500 – 2.600	0.3339	$\pm 0.0243$

**Table 3.** Total cross sections of the reaction  $\gamma p \rightarrow K^+ \Sigma^+ \pi^-$  with  $\Sigma^+ \rightarrow n\pi^+$  for 13 bins of  $E_\gamma$ , obtained after background subtraction.

$E_\gamma$ [GeV]	$\sigma_{tot}$ [ $\mu\text{b}$ ]	$\delta\sigma$ [ $\mu\text{b}$ ]
1.300 – 1.400	0.0116	$\pm 0.0076$
1.400 – 1.500	0.0720	$\pm 0.0191$
1.500 – 1.600	0.1644	$\pm 0.0275$
1.600 – 1.700	0.2314	$\pm 0.0419$
1.700 – 1.800	0.4005	$\pm 0.0359$
1.800 – 1.900	0.5377	$\pm 0.0448$
1.900 – 1.000	0.7802	$\pm 0.0559$
2.000 – 1.100	0.6789	$\pm 0.0641$
2.100 – 2.200	0.6861	$\pm 0.0650$
2.200 – 2.300	0.8147	$\pm 0.0726$
2.300 – 2.400	0.9029	$\pm 0.0894$
2.400 – 2.500	0.6359	$\pm 0.0806$
2.500 – 2.600	0.7302	$\pm 0.0868$

**Table 4.** Total cross sections of the reaction  $\gamma p \rightarrow K^+ \Sigma^+ \pi^-$  with  $\Sigma^+ \rightarrow p\pi^0$  for 13 bins of  $E_\gamma$ , obtained after background subtraction.

$E_\gamma$ [GeV]	$\sigma_{tot}$ [ $\mu\text{b}$ ]	$\delta\sigma$
1.300 – 1.400	0.0067	$\pm 0.0113$
1.400 – 1.500	0.0367	$\pm 0.0347$
1.500 – 1.600	0.1075	$\pm 0.0538$
1.600 – 1.700	0.3395	$\pm 0.0496$
1.700 – 1.800	0.3817	$\pm 0.0519$
1.800 – 1.900	0.5983	$\pm 0.0605$
1.900 – 1.000	0.7209	$\pm 0.0662$
2.000 – 1.100	0.7605	$\pm 0.0794$
2.100 – 2.200	0.9128	$\pm 0.0662$
2.200 – 2.300	0.9323	$\pm 0.0816$
2.300 – 2.400	0.8905	$\pm 0.1151$
2.400 – 2.500	0.7702	$\pm 0.1115$
2.500 – 2.600	0.9037	$\pm 0.$

structure of nucleons and nuclei with electromagnetic probes’’ (SPP 1034 KL 980/2-3) and the Sonderforschungsbereich SFB/TR16 (‘‘Subnuclear Structure of Matter’’).

## References

1. E. Klempt, J.-M. Richard, Rev. Mod. Phys. 82, 10951153 (2010).
2. K.-H. Glander *et al.*, Eur. Phys. J. A 19, 251 (2004).
3. S. Goers *et al.*, Phys. Lett. B 464, 331 (1999).
4. R. Lawall *et al.*, Eur. Phys. J. A 24, 275 (2005).
5. C. Wu *et al.*: Eur. Phys. J. A 23 (2) (2005).
6. J. Barth *et al.*: Eur. Phys. J. A 18 117-127 (2003).
7. J. Barth *et al.*: Eur. Phys. J. A 17 2, 269-274 (2003).
8. R. Plötzke *et al.*: Phys. Lett. B 444 555-562 (1998).
9. W. J. Schuille *et al.*, Nucl. Instr. Meth. A 344, 470 (1994).
10. W. Hillert, Eur. Phys. J. A28, 139 (2006).
11. F. W. Wieland *et al.*, preceding paper.
12. R. Erbe *et al.* (ABBHHM), Physical Review 188, 2060 (1969).
13. S. Goers, doctoral thesis, Bonn University (1999), BONN-IR-1999-09.
14. B. Krusche *et al.*, Phys. Rev. Lett. **74**, 3736 (1995).
15. A. Bleckmann *et al.*, Z. Phys. **239**, 1 (1970).
16. R. Bradford *et al.*, Phys. Rev. C 73, 035202 (2006).